Characterization and Properties of Polypropylene-*block*-poly(ethylene-*co*-propylene) Synthesized by Short-Period Polymerization

KOH-HEI NITTA,[1] TAKENORI KAWADA,[1] VALERY V. PROKHOROV,[1] MIKIO YAMAHIRO,[2] HIDEHARU MORI,[2] MINORU TERANO[2]

[1] Center for New Materials, Japan Advanced Institute of Science and Technology,
1-1 Asahidai, Tatsunokuchi, Ishikawa 923-1292 Japan

[2] School of Materials Science, Japan Advanced Institute of Science and Technology,
1-1 Asahidai, Tatsunokuchi, Ishikawa 923-1292 Japan

Received 2 September 1998; accepted 28 February 1999

ABSTRACT: The morphology and mechanical properties of novel block copolymers consisting of isotactic polypropylene (PP) and ethylene–propylene rubber (EPR) synthesized by a short-period polymerization method were examined using differential scanning calorimetry, atomic force microscopy, dynamic mechanical analysis, and a rheooptical technique. It was found that the novel block copolymers show a single glass transition and EPR segments are trapped into the amorphous region of PP. Furthermore, the rheooptical analysis demonstrates that a drawing process of the EPR-rich block copolymer induces orientation of the PP lamellae in the EPR matrix. © 1999 John Wiley & Sons, Inc. J Appl Polym Sci 74: 958–964, 1999

Key words: polypropylene; ethylene–propylene copolymer; diblock copolymer; rheooptical properties; mechanical properties

INTRODUCTION

In a previous paper,[1] we demonstrated the possibility of preparing diblock copolymers of isotactic polypropylene (designated as PP) and ethylene–propylene random copolymer (designated as EPR) with a short-period polymerization method. It was determined that the short-period (or stopped-flow) polymerization makes it possible to perform "quasiliving polymerization" during a very short period (up to about 0.2 s) in such a way of avoiding chain-transfer reactions.[2–4] The formation of a block structure, in which EPR is chemically linked with PP, has been suggested from the experimental facts[1] that molecular distribution curves in gel-permeation chromatography (GPC) are unimodal and the EPR component exists on ^{13}C-NMR spectra after extraction with heptane.

The block copolymers of PP and EPR have been assumed to have the potential of improving the low-temperature toughness of PP.[5–7] Very little is known, however, regarding the morphology, thermal behavior, and mechanical properties of diblock copolymers of PP and EPR because of the lack of complete diblock copolymers of PP and EPR. In this work, we examined the morphological characteristics and the melting and mechanical behaviors of the present copolymers using atomic force microscopy, differential scanning calorimetry, dynamic mechanical analysis, and infrared dichroism in combination with stress–strain measurements.

Correspondence to: K. Nitta.

Contract grant sponsor: TOSOH Corp.

Journal of Applied Polymer Science, Vol. 74, 958–964 (1999)

CCC 0021-8995/99/040958-07

Table I Characterization of Polymers

Polymer	Composition PP	Composition EPR	$M_w{}^a \times 10^{-4}$	$M_w/M_n{}^a$	Ethylene[b] Content (mol %)	T_m (K)	Density (kg m^{-3})	Crystal Form
PP	100	—	2.9	3.0	—	435	911	Monoclinic
EPR	—	100	3.2	3.3	39.5	—	870	—
PP-*b*-EPR	75	25	5.1	3.2	17.2	434	899	Monoclinic
PP-*b*-EPR	50	50	4.2	3.0	25.7	433	892	Monoclinic
PP-*b*-EPR	25	75	3.6	3.0	29.7	428	886	Monoclinic

[a] Determined by gel permeation chromatography, PP standard.
[b] Determined by ^{13}C-NMR.

EXPERIMENTAL

Materials

The block copolymers of PP and EPR (designated as PP-*b*-EPR) were synthesized by a short-period polymerization method. The polymerization was carried out for about 0.1 s with a $MgCl_2$-supported Ziegler catalyst in toluene at 303 K. The length of each sequence was controlled by changing the polymerization times. For comparison, the PP homopolymer and EPR copolymer were also prepared using the same polymerization process. Details of the polymerization procedure were shown in the previous paper.[1]

The molecular characteristics of the polymers used in this study are summarized in Table I. The molecular weight and its distribution were determined using a high-temperature GPC instrument (Senshu SSC-7100) with *o*-dichlorobenzene (ODCB) as a solvent at 413 K. The ethylene content in the samples was determined by ^{13}C-NMR spectra using a Varian Gemini-300 spectrometer.

Sample Preparation and Characterization

For the mechanical measurements, the samples were melt-pressed in a laboratory hot press at 463 K and at 12 MPa. The film specimens were prepared by quenching from the melts into an ice-water bath. The thickness of the compression-molded films was adjusted to a suitable thickness to suit the intended experiment. The results of the film characterization are also included in Table I.

The crystal form of the film specimens which were used for the mechanical measurements was examined by wide-angle X-ray diffraction (WAXD). The measurements were carried out at a scanning speed of 1°/min over a 2θ range from 8° to 40° using a WAXD instrument (Rigaku RINT-2000).

Densities of the specimens were determined by a floatation method.[8] A binary medium prepared from various ratios of distilled water and ethyl alcohol was used.

DSC measurements were carried out using a Mettler Tredo calorimeter DSC820 that was calibrated for temperature and melting enthalpy using indium as a standard. The samples of about 10 mg weight sealed in aluminum pans were used for the measurements. The samples were heated from 170 to 500 K at a scanning rate of 10 K/min under a nitrogen atmosphere.

Measurements

Mechanical Properties

The measurements of the linear dynamic mechanical properties were made using a dynamic mechanical analyzer (Rheology DVE-V4) on film specimens of the following dimensions: length 20 mm, width 5 mm, and thickness 0.3 mm. The dynamic tensile moduli, the storage modulus E', the loss modulus E'', and the loss tangent tanδ ($=E''/E'$) were measured between 120 to 430 K at a constant frequency of 10 Hz and a heating rate of 2 K/min.

We have developed a rheooptical system[9–12] to elucidate the deformation mechanism for film specimens. In the present study, infrared dichroism was measured simultaneously with the tensile load during stretching of the film specimen. The apparatus is based on a previous one described elsewhere.[12]

A tensile tester was set in a Fourier-transform infrared (FTIR) spectrometer (JASCO FT-IR500) in such a way as to allow an infrared beam to go through a central point of the film mounted on the tensile tester. The tensile tester was designed for upper and lower clamps to symmetrically move from the central point or the beam point in the film. The film specimens were cut into a dumbbell shape with 100 μm thickness in which the gauge length was 10 mm. The tensile strain was calculated from the ratio of the increment of the length between clamps to the initial gauge length. The tensile stress was determined by dividing the tensile load by the initial cross section. The crosshead speed was 1 mm/min in all cases.

The orientation function of the *c* crystallographic axis (*c*-axis) with respect to the stretching direction for PP can be determined from the dichroic ratio *D* for the 998 cm^{-1} absorption band.[13,14]

Supermolecular Structure

The spherulitic and lamellar morphologies were investigated using an Olympus DP-10 polarizing optical microscope (POM) and a Digital Instruments Nanoscope III multimode atomic force microscope (AFM). The AFM applied in the tapping mode[15] was used with integrated silicon tips and cantilevers with a nominal spring constant of 30 N/m. Height, amplitude, and phase data were recorded. Of these three types, the phase images had usually the finest details of the surface structure for the samples prepared by the below procedure.

To examine the morphological feature and characteristics of the PP-*b*-EPR samples, we prepared the samples using the following experimental procedure: One to two drops of the polymer samples dissolved in the ODCB solution at a concentration of 0.5% were deposited on the surface of glass slides placed on the hot stage at the temperature 410–430 K. After the evaporation of the solvent during, in 1 min, the thin films were placed in the another hot stage at 400 K for crystallization for a time in the range of 10–30 min. Some commercial antioxidants were used with the concentration in the dry polymer samples of 0.1%.

RESULTS AND DISCUSSION

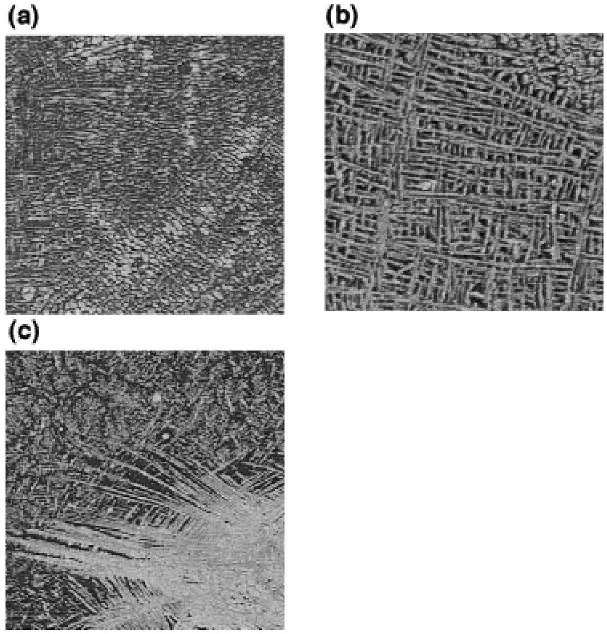

Figure 1 AFM phase images of (a) PP-*b*-EPR(75–25); (b) PP-*b*-EPR(50–50); and (c) PP-*b*-EPR(25–75). The scan size is 2 μm for the (a) and (b) images, and 8 μm for (c) image. Contrast (from dark to bright) covers the height variations of phase angle in the range of 15° for (a) and (b) images, and 90° for (c) image.

Figure 1 represents the AFM phase images of the prepared samples' regions with pronounced lamellar structure. The crosshatching, which is typical for quadrite structures,[16] and the α-form spherulites as seen in the PP[17] homopolymer may be clearly seen for all three PP-*b*-EPR samples. The POM images of three block copolymers were poorly pronounced and contained usually no sharp boundaries between the spherulites which were of a small size (10–20 μm). It was possible, nevertheless, to determine that the sign of birefringence for all the structures was always positive. This fact suggests the existence of a well-developed cross-hatching structure with the characteristic angle of 80°, resulting in positive birefringence.[17] It may be seen also that the long period, L_p, of these structures monotonically increases with increase of the EPR weight fraction: These values are about 25 ± 5, 40 ± 10, and 60 ± 20 nm for the PP-*b*-EPR samples with an EPR content 25, 50, and 75%, respectively. It should be noted here that the average values from AFM may not the same as in the bulk because the AFM images basically reflect the lamellar morphology on the surface.[18]

A relatively large dispersion of L_p is noticed for the PP-*b*-EPR(25-75) sample, due to that lamellae or lamellar agglomerates are randomly dispersed in the noncrystalline matrix. One more important result concerning the difference in phase images among these three block samples is that the phase contrast of the PP-*b*-EPR(25–75) covers the range of about 70° in comparison to 10°–12° for the PP-*b*-EPR(75–25) and PP-*b*-EPR(50–50) images. This fact suggests that the PP-*b*-EPR(25—75) shows a much greater energy dissipation during scanning[19] on the amorphous EPR regions [dark portions in Fig. 1(c)] because of its higher EPR content.

These surface morphological features of PP-*b*-EPR may be due to that the crystallizable PP part is linked with the noncrystallizable EPR part. However, the morphology profile will be dependent on the crystallization processes such as the crystallization temperature and time. Details of the crystallization mechanism of these block copolymers will be reported in the near future.

The melting behavior was investigated by DSC at a rate of 10 K/min on the PP and various PP-*b*-EPR samples crystallized at different cooling rates from −20 to −1 K/min. As shown in Figure 2, the PP and PP-*b*-EPR(75–25) block films which have been rapidly cooled exhibit a lower melting temperature and bimodal melting. At lower cooling rates, the crystal thickening occurs, leading to more perfect crystals due to time for the reorganization or rearrangement of the PP crystals. A similar result is commonly observed for other melt-crystallized polymers as well as for the PP/EPR blends. Oppositely, for the PP-*b*-EPR(50–50) and PP-*b*-EPR(25–75) blocks (see Fig. 3), the slow-cooled state has thinner crystals to a much greater extent than the quenched state.

Recent experimental[20–24] and theoretical[25,26] studies have demonstrated that an equilibrium morphology of crystalline–amorphous diblock copolymers, having relatively low molecular weight, is thermodynamically favorable for the accommodation of the amorphous component to reside between lamellae. This is because the free-energy reduction is not so large such that crystallization can readily overcome the energy barrier to disrupt the phase-separated morphology.[21,22]

In the case of the EPR-rich blocks, the slow-cooled procedure induces aggregation of the EPR phase and this leads to a disturbance of the recrystallization or rearrangement process of the PP crystal. In other words, the crystalline state is disturbed by the segregation process of incompatible components that are chemically linked. On the other hand, the reorganization of the PP crystals in the "PP-rich" block film overcomes the segregation process of the PP and EPR components because of the longer crystallizable PP block. Consequently, such competitive effects of crystallization and phase separation seem to be associated with the block formation of the present copolymers prepared by the short-period polymerization method.

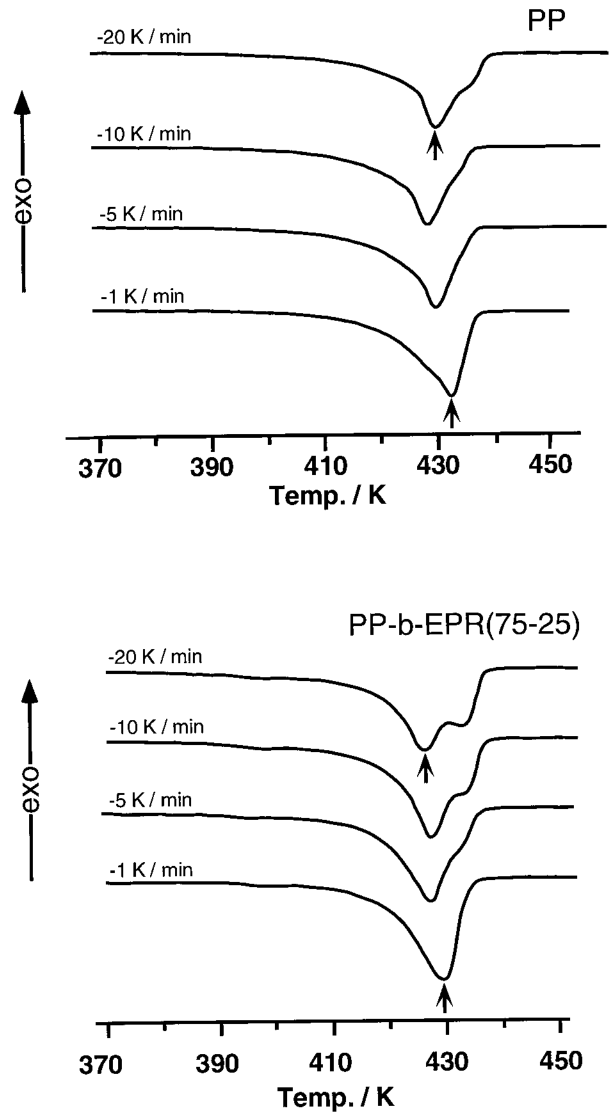

Figure 2 DSC melting thermograms of PP and PP-*b*-EPR(75–25) block copolymer measured on heating rate of 10 K/min. The samples are prepared by cooling rates of −1, −5, −10, and −20 K/min.

The temperature dependencies of E' and E'' of the PP-*b*-EPR(50–50) block film are shown in Figure 4. For comparison, the dynamic mechanical spectra of the PP and EPR samples prepared using the present equipment (see Table I) are also added to this figure. As is well known, the PP/EPR blend films have a phase-separated morphology so that there are apparently two peaks of E'' in the temperature range from 200 to 300 K, in

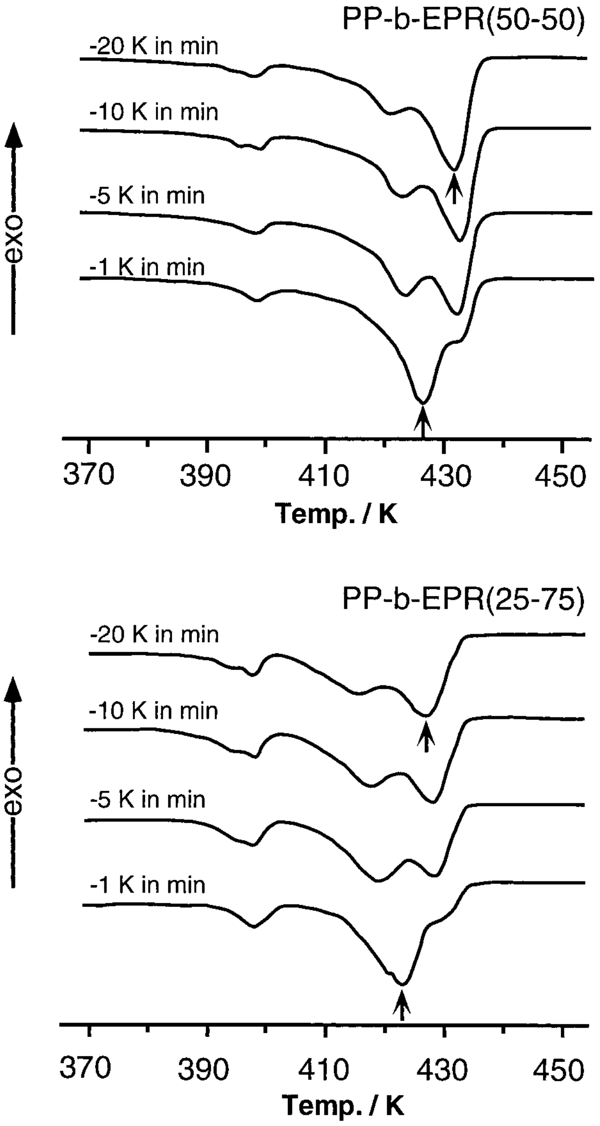

Figure 3 DSC melting thermograms of PP-*b*-EPR(50–50) and PP-*b*-EPR(25–75) block copolymers measured on heating rate of 10 K/min. The samples are prepared by cooling rates of −1, −5, −10, and −20 K/min.

which the higher-temperature peak at around 275 K corresponds to the glass transition, T_g, of the amorphous region of PP, and the lower relaxation peak around 220 K corresponds to the T_g of the EPR component.[27] The present block copolymers, having no macroscopical phase separation, show a very broad relaxation peak between the two relaxation peaks of the PP and EPR segments in the dynamic mechanical spectra, which are reminiscent of the characteristics of the compatible blends.[27] In addition, it was found that the activation energy of the relaxation process for

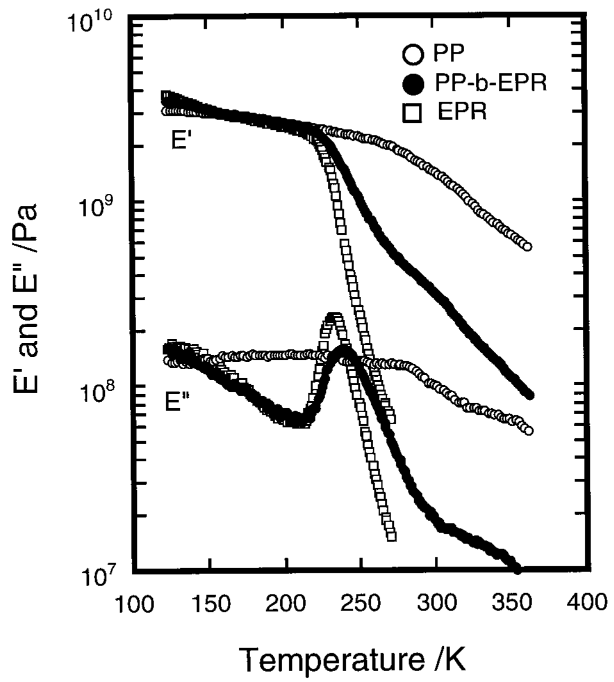

Figure 4 Temperature dependence of mechanical storage modulus (E') and loss modulus (E'') at 10 Hz for a quenched PP-*b*-EPR(50–50), PP, and EPR films.

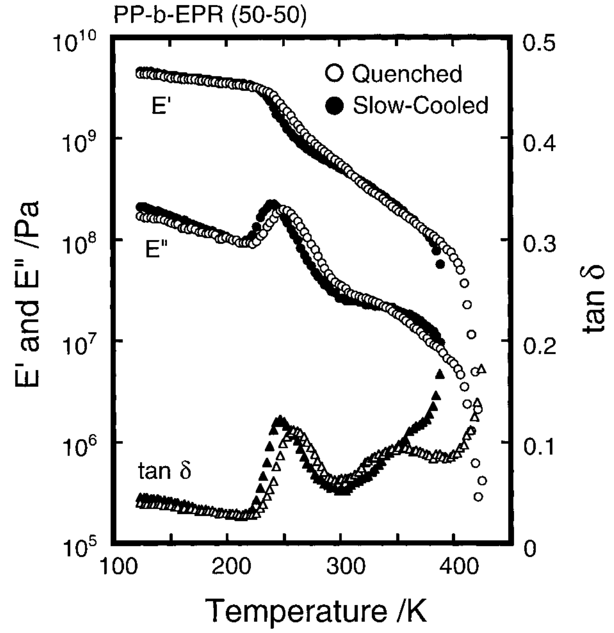

Figure 5 Comparison of temperature dependence of mechanical storage modulus (E'), loss modulus (E''), and loss tangent (tanδ) at 10 Hz between a slow-cooled PP-*b*-EPR(50–50) film (closed symbols) and a quenched PP-*b*-EPR film (open symbols).

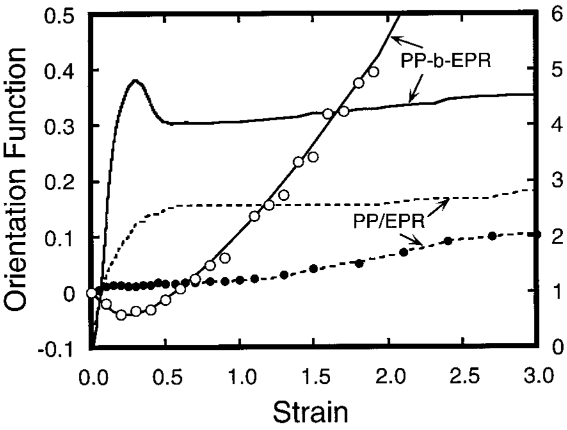

Figure 6 Strain dependence of orientation function (○) for the 998 cm^{-1} band and the stress–strain curve (solid line) for PP-*b*-EPR(25–75) film, including the orientation function (●) and stress–strain curve (dotted line) for a binary (25/75) blend of commercial PP and EPR grades.[27]

PP-*b*-EPR was 230 kJ/mol, which is intermediate between those of PP (270 kJ/mol) and EPR (210 kJ/mol). According to transmission electron microscopy observations, the PP-*b*-EPR block film was also found to exhibit no phase separation as seen in the PP/ERP belnds.[27] These results indicate that the EPR molecules are trapped into the amorphous region of PP.

To examine the annealing effect of the dynamic mechanical behavior, we prepared a slow-cooled PP-*b*-EPR block film which was crystallized by at cooling rate of 2 K/min in a hot press. Figure 5 compares the dynamic mechanical spectra of quenched and slow-cooled PP-*b*-EPR(50–50) films. The T_g relaxation peak of the slow-cooled films was found to be shifted to a lower temperature than that of the quenched one. Furthermore, a broad dispersion in the range from 300 to 400 K, which is ascribed to intracrystalline chain motion and rearrangement of the slow-cooled PP-*b*-EPR(50–50) film, shows a slightly lower temperature shift than that of the quenched film. Oppositely, as is typical for semicrystalline polymers, but not presented here, the slowly cooled crystallization process leads to a shift of these dispersions of PP and "PP-rich" PP-*b*-EPR(75–25) block films to higher temperatures. These annealing effects of the dynamic mechanical spectra also suggest that the EPR molecules are trapped into the amorphous region of PP.

The orientation behavior of the chain axis (*c*-axis) in the crystalline region was investigated by a simultaneous measurement of the tensile load and infrared spectra as a function of the strain or elongation time. The rheooptical results of PP-*b*-EPR(25–75) are shown in Figure 6. The other block samples such as PP-*b*-EPR(75–25) and PP-*b*-EPR(50–50) were too brittle to be elongated for the rheooptical measurements. The drawability of the PP-*b*-EPR(25–75) film is due to that the PP phases are surrounded by the rubbery EPR matrix. For comparison, the data for the binary blend of PP and EPR, which are commercial grades, are also shown in Figure 6.

As seen in Figure 6, the elongation of the PP-*b*-EPR film induces the orientation of the PP chains and this leads to a yield point in the stress–strain curve despite of its higher EPR content. It is of interest to note that the yield stress of PP/EPR(25/75) is one order of magnitude less than that of typical PP homopolymers, yet PP/EPR(25/75) showed no yield point and no PP orientation. The deformation and orientation behavior of PP-*b*-EPR(25–75) mean that the external force exerts directly on the PP phase through the matrix EPR segments. This suggests that the PP part is chemically linked with the EPR part, because PP-*b*-EPR(25–75) displays a clear yield point, and its stress–strain curve is similar in shape to the curve of PP homopolymers. The PP-*b*-EPR shows a negative *c*-axis orientation in the initial strain region. The magnitude and the strain region of the negative *c*-axis orientation are much greater than those of PP homopolymers.[12] This is due to that the lamellar orientation and rotation forced by deformed EPR parts cause the chain axis in the PP crystals (*c*-axis) to orient perpendicular to the stretching direction. In the higher-strain region, the rotation and orientation of the fragmented lamellae occurs beyond the yield process so that the orientation of the *c*-axis becomes progressively greater with increasing strain.

CONCLUSIONS

Some novel block copolymers consisting of PP and EPR sequences were synthesized by a short-period polymerization method. In the present study, the DSC thermograms, AFM observation, dynamic mechanical spectra, and rheooptical properties for the novel block copolymers were investigated. These experimental results supported the block formation of the novel copolymers. It should be noted that the molecular basis of the mechanical properties of the novel block copolymers is much different from that of the corresponding blends. This indicates that the addition of the copolymers has a potential to modify the mechanical properties of PP/EPR blends. Accordingly, it is very interesting to examine whether the present block copolymers can be used as compatibilizing agents for PP and EPR blends. In the near future, the additive effects of the block copolymer on the tensile properties of PP/EPR blends will be reported.

The authors thank Dr. Hisayuki Nakatani and Mr. Osamu Notoya of the Center for New Materials, JAIST, for assistance with the TEM observations. Furthermore, one of the authors (K.N.) would like to express his sincere thanks to Prof. Motowo Takayanagi of Kyushu University for his valuable discussions and suggestions and deeply appreciates the financial support to our laboratory by TOSOH Corp.

REFERENCES

1. Mori, H.; Yamahiro, M.; Tashino, K.; Ohnishi, K.; Nitta, K.; Terano, M. Macromol Chem Rapid Commun 1995, 16, 247.
2. Keii, T.; Terano, M.; Kimura, K.; Ishii, K. Makromol Chem Rapid Commun 1987, 8, 583.
3. Terano, M.; Kataoka, T.; Keii, T. J Mol Catal 1989, 56, 203.
4. Keii, T.; Terano, M.; Kimura, K.; Ishii, K. In Transition Metals and Organometallics as Catalysts for Olefin Polymerization; Kamminsky, W.; Sinn, H., Eds.; Springer-Verlag: Berlin, Heidelberg ,1988; p 1.
5. Wilkes, G. L.; Mody, P. C.; Tant, M. R. Polym Eng Sci 1979, 19, 1029.
6. Takahashi, T.; Mizuno, H.; Thomas, E. L. J Macromol Sci-Phys B 1983, 22, 425.
7. Wang, L.; Huang, B. J Polym Sci Part B Polym Phys 1991, 29, 1447.
8. Roberts, R. M.; Gilbeit, J. C.; Lodgeward, L. B.; Wingrove, A. S. In An Introduction to Moden Experimental Organic Chemistry; Holt Rinehart and Winston: New York, 1969.
9. Stein, R. S. In New Method of Polymer Characterization; Ke, B., Ed.; Wiley: New York, 1968; p 255.
10. Wilkes, G. L. Adv Polym Sci 1971, 8, 91.
11. Onogi, S.; Asada, T.; Sakai, K. Proc 5th Int Cong Rheol 1970, 4, 41.
12. Nitta, K.; Okamoto, K.; Yamaguchi, M. Polymer 1998, 39, 53.
13. Read, B. E. In Structure and Properties of Oriented Polymers; Ward, I. M., Ed.; Applied Science: London, 1975; p150.
14. Onogio, S.; Asada, T.; Tanaka, A. J Polym Sci A-2 1969, 7, 171.
15. Zhong, Q.; Innis, D.; Kjoller, K.; Ellings, V. Surf Sci Lett 1993, 290, 688.
16. Khoury, F. J Res Natl Bur Stand A 1966, 70, 29.
17. Norton, D. R.; Keller, A. Polymer 1985, 26, 704.
18. Zhou, H.; Wilkes, G. L. Polymer 1997, 38, 5735.
19. Cleveland, J. P.; Anczykowski, B.; Schmid, A. E.; Elings, V. B. Appl Phys Lett 1998, 72, 2613.
20. Unger, R.; Beyer, D.; Donth, E. Polymer 1991, 32, 3305.
21. Nojima, S.; Kato, K.; Yamamoto, S.; Ashida, T. Macromolecules 1992, 25, 2237.
22. Rangarajan, P.; Register, R. A.; Fetter, L. J. Macromolecules 1993, 26, 4840.
23. Ryan, A. J.; Hamley, I. W.; Bras, W.; Bates, F. S. Macromolecules 1995, 28, 3860.
24. Lovinger, A. J.; Han, B. J.; Padden, F. J.; Mirau, P. A. J Polym Sci Part B Polym Phys 1993, 31, 115.
25. DiMarzio, E. A.; Guttman, C. M.; Hoffman, J. D. Macromolecules 1980, 13, 1194.
26. Whitmore, M. D.; Noolandim, J. Macromolecules 1988, 21, 1482.
27. Yamaguchi, M.; Miyata, H.; Nitta, K. J Appl Polym Sci 1996, 62, 87.